ISS RADIATION ENVIRONMENT AS OBSERVED BY LIULIN TYPE-R3DR2 INSTRUMENT IN OCTOBER-NOVEMBER 2014

Tsvetan Dachev[1], Borislav Tomov[1], Yury Matviichuk[1], Plamen Dimitrov[1], Nikolay Bankov[1], Donat-Peter Häder[2], Gerda Horneck[3], Günter Reitz[3]

[1]Space Research and Technology Institute – Bulgarian Academy of Sciences
e-mail: tdachev@bas.bg
[2]Neue Str. 9, 91096 Möhrendorf, Germany; e-mail: donat@dphaeder.de
[3]DLR, Institute of Aerospace Medicine, Köln, Germany
e-mail: gerda.horneck@dlr.de, Guenther.Reitz@dlr.de

Abstract

Space radiation was monitored using the R3DR2 spectrometer-dosimeter during the flight outside the Russian "Zvezda" module of ISS in October-November 2014. The instrument was mounted on the ESA EXPOSE-R2 platform. The R3DR2 instrument was first developed and used during the flight of ESA EXPOSE-R platform in 2009-2010 (Dachev et al, 2015a). It is a low mass, small dimension automated device that measures solar visible and ultraviolet (UV) radiation in four channels and ionizing radiation in 256 channels of a Liulin-type energy deposition spectrometer (Dachev et al, 2002). Ionizing radiation was measured and separated in 256 deposited energy spectra, which were further used for determination of the absorbed dose rate and flux. The main results obtained by the R3DR2 instrument are: (1) three different radiation sources were detected and quantified - galactic cosmic rays (GCR), energetic protons from the inner radiation belt (IRB) in the region of the South Atlantic anomaly and energetic electrons from the outer radiation belt (ORB); (2) for the first time in the history of using of the Liulin-type energy deposition spectrometers (Dachev et al, 2015b) an observable flux from solar energetic particles (SEP) was detected in the period 1-4 November 2014; (3) the obtained SEP energy deposition spectra were compared with other spectra to confirm their shape.*

Introduction

This paper analyses the results for the space radiation environment outside the Russian "Zvezda" module of ISS generated by different radiation sources including: Galactic Cosmic Rays (GCR), Inner Radiation Belt (IRB) trapped protons in the region of the South Atlantic Anomaly (SAA) and Outer Radiation Belt (ORB) relativistic electrons. Low intensity Solar energetic particles (SEP) were observed in the 1-2 November time interval. In addition, there is secondary radiation produced in the shielding materials of the ESA EXPOSE-R2 platform and Russian "Zvezda" module. Dose characteristics in the R3DR2 instrument also depend on many other variables such as the ISS orbit parameters, solar cycle phase and current helio- and geophysical activity. In this study the orbital parameters were calculated by the software KADR-2 (Galperin et al., 1980). More comprehensive information for the ISS radiation environment was published in the recently overview by Dachev et al. (2015b).

Materials and methods

R3DR2 instrument description

In order to determine and quantify the radiation field outside the ISS, in the ESA EXPOSE-E/R platform, a radiation environment spectrometer-dosimeters R3DE/R was developed through collaboration of the Bulgarian and German teams (Streb et al., 2002; Häder and Dachev 2003; Häder et al., 2009). The teams worked successfully during the ESA EXPOSE-E/R missions in 2008-2009 and 2009-2010 time periods, respectively. The currently used R3DR2 spectrometer-dosimeter on the ISS is in fact the same instrument which was flown in 2009-2010 in the EXPOSE-R facility but here it is named with the extension R2 only for purposes to distinguish between the data from the different EXPOSE-R(1) and EXPOSE-R2 missions.

The R3DR2 is a Liulin-type instrument which was successfully flown: 1) In the USA Laboratory module of the ISS in May-August 1991 (Reitz et al., 2005; Dachev et al., 2002; Nealy et al., 2007; Wilson et a.l, 2007; Slaba et al., 2011, Badavi, 2014); 2) Inside ESA Biopan-5/6 facilities on Foton M2/M3 satellites in 2005/2007 (Häder et al., 2009; Damasso et al., 2009); 3) Inside the ESA EXPOSE-E/R facilities outside the Columbus/Zvezda modules of the ISS in 2008-2010 (Dachev et al., 2012a; Dachev et al., 2015a).

The scientific objectives of the RDR2 spectrometer-dosimeter exposure were: first connected with the quantification of the global distribution and time
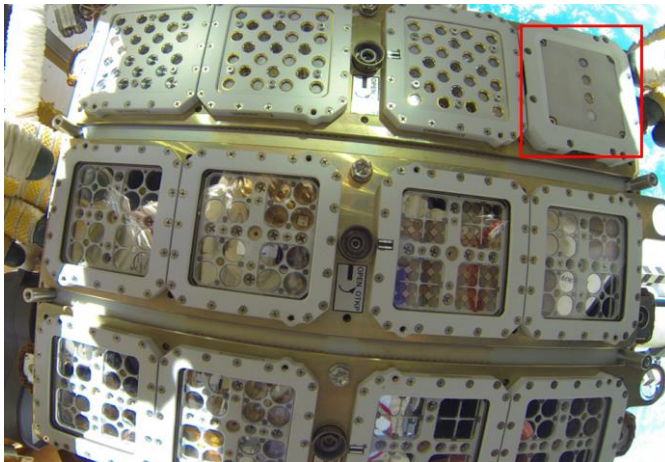
Fig. 1. External view of R3DER instrument (in the red square) as mounted in the EXPOSE-R2 facility. (Picture taken by Russian cosmonaut Aleksandr Samokutyaev on 22 October 2014 during EVA-2 for mounting of EXPOSE-R2 facility outside Russian "Zvezda" module. (Picture credit of ESA/NASA/RKA)

dynamics of the radiation fields, generated by different radiation sources outside the ISS; the second purpose is the dosimetric support for other passive scientific experiments, related to astrobiology (Rabbow et al., 2015), which were housed

inside the EXPOSE-R2 facility. For all of these experiments the knowledge of the history of solar and ionizing radiation and the total obtained doses is highly important for the interpretation of the data collected during the mission.

Figure 1 presents the external view of the R3DR2 instrument as mounted in the EXPOSE-R2 facility. The R3DR2 instrument is a low mass, small dimension automatic device that measures solar radiation in four channels and ionizing radiation in 256 channels of a Liulin-type energy deposition spectrometer (Dachev et al., 2015b). The four solar UV and visible radiation photodiodes are seen as small circles on the surface in the central part the R3DR instrument. The ionizing radiation detector is located behind the aluminum wall of the instrument and is not seen in the figure. The aluminum box of R3DR instruments has a size of 76×76×34 mm and weight of 120 g.

The cosmic radiation is determined using a semiconductor detector (2 cm^2 area and 0.3 mm thick). A pulse height analysis technique is used to measure the deposited energies (doses) in the detector. Charge pulses generated in the detector are preamplified and then passed to the discriminator. The amplitudes of the pulses are detected and converted into digital signals by a 12 bit analog to digital converter (ADC), which are subsequently sorted into a 256 channels spectrum according to their amplitudes by a multi-channel analyzer (MCA). One energy deposition spectrum is accumulated over 10 s. The 256th energy channel stores all pulses with amplitudes higher than the sensitivity range (19.5 mV–5.0 V) of the detector, which corresponds to the energy deposition range (0.081-20.83 MeV).

The dose D [Gy] by definition is one Joule deposited in 1 kg of matter. We calculate the absorbed dose in the silicon of the detector by dividing the summarized energy deposition in the spectrum in Joules by the mass of the detector in kilograms.

$$(1) \qquad D = K \sum_{i=1}^{255} i k_i A_i M D^{-1},$$

where MD is the mass of the detector in kilograms (kg), k_i is the number of pulses in channel "i", A_i is the amplitude in Volts (V) of pulses in channel "i", $i.k_i.A_i$ is the deposited energy (energy loss) in Joules (J) in channel "i" and K is a coefficient. Incoming space radiation sources are characterized using the methods described by Dachev (2009).

Instrument calibrations

The R3DR2 instruments were calibrated in a wide range of radiation fields. First, they were irradiated in gamma and neutron (^{137}Cs, ^{60}Co, AmBe and ^{252}Cf) isotope sources radiation fields and at the CERN-EC high energy reference field (Spurny and Dachev, 2003, Dachev et al., 2002). The absolute values of the dose rates obtained from the spectrometer are in very good agreement with the dose rates calculated using the EGS4 transport code (http://rcwww.kek.jp/research/egs/). The values of the measured doses were found to be within 2.8% of the reference

value for the ^{137}Cs source and within 8% of the ^{60}Co source (Spurny and Dachev, 2003). The calibrations showed that the spectrometer had high effectiveness with respect to gamma rays, which allowed monitoring of the natural background radiation. Next, the Liulin type spectrometer was calibrated at the cyclotron at Universite Catholique de Louvain, Louvain-la-Neuve, Belgium (Dachev et al., 2002) and by using proton and heavy ion beams in the National institute for radiological sciences (NIRS) Cyclotron facility and the HIMAC heavy ion synchrotron facility at NIRS, Chiba, Japan (Uchihori at al., 2002, 2008). All calibration results and also the GEANT-4 and PHITS code simulations (Ploc et al., 2011) revealed very good coincidence between the measured and predicted energy deposition spectra and proved the effectiveness of the Liulin spectrometers for the purposes of characterization of the space radiation field (Uchihori at al., 2008). A recent review paper (Dachev et al. 2015b) gives a comprehensive description of the Liulin type spectrometers developed since 1996 and their calibrations and space results.

The DES effectiveness for neutrons depends on their energy, being minimal for neutrons with energy of 0.5 MeV and having a maximum of a few percent for neutrons with energies of 50 MeV. According to the "neutron-induced nuclear counter effect" introduced for the Hamamatsu PIN diodes of type S2744-08 (Zhang et al., 2011). Almost all DESs used the same type PIN diodes, and neutrons could be observed in all channels of the spectrum with a higher probability in the first 14 channels.

The ionizing radiation detector of the R3DR2 instrument was mounted about 3 mm below the 1 mm thick aluminium cover plate. Additionally, there was a technological shielding of 0.2 mm copper and 0.2 mm plastic material, resulting in less than 0.6 g cm^{-2} total shielding. This allows the measurement of direct hits by electrons with energies higher than 1.18 MeV and by protons with energies higher than 27.5 MeV (Berger, 2014).

Data analysis and results
All data presentation

The first month (24 October-25 November 2014) of EXPOSE-R2 active data collection mission took place in the middle phase of the 24th solar cycle after the secondary maximum in 2014 (http://www.swpc.noaa.gov/products/solar-cycle-progression). One relatively small solar energetic proton (SEP) event was measured by the R3DR2 instrument, the maximum of which occurred about 22:00 h UTC on 3 November 2014 in the GOES 15 "Space Environment Monitor (SEM)" (http://goes.gsfc.nasa.gov/text/databook/section05.pdf, 30 MeV channel data). No real enhancement in the GOES 15 proton flux with energies above 100 MeV was observed (ftp://ftp.swpc.noaa.gov/pub/warehouse/2014). The geomagnetic field during the period of the ISS flight was at a moderate level with two "strong" and one "moderate" (http://www.swpc.noaa.gov/noaa-scales-explanation) geomagnetic storms on 4, 10 and 16 November 2014. The global

geomagnetic storm index Kp (Bartels et al., 1939) reached three noticeable maxima: The first with a maximum of Kp=6 in the interval 09:00-12:00 UT on 4 November 2014; the second maximum with a Kp=7 in the interval 09:00-12:00 UT on 10 November 2014; a third maximum with a Kp=7 in the interval 09:00-12:00 UT on 16 November 2014 (ftp://ftp.swpc.noaa.gov/pub/warehouse/2014).

Radiation sources selection procedures

The following four expected radiation sources can be detected in the data obtained with the R3DR2 instrument: (i) globally distributed GCR particles and their secondaries; (ii) protons with more than 27.5 MeV energy in the SAA region of the IRB; (iii) relativistic electrons and/or *bremsstrahlung* with energies above 1.18 MeV in the high latitudes of the ISS orbit where the ORB is situated; (iv) solar energetic protons (SEP) in the high latitudes of the ISS orbit.

Historically we developed two similar radiation source data selection procedures. The simplest method to distinguish between the contribution of the IRB protons and the ORB electrons is based on the Heffner formulae (Heffner, 1971; Dachev, 2009), which uses the dose to flux ratio (D/F) or the specific dose (SD). When the
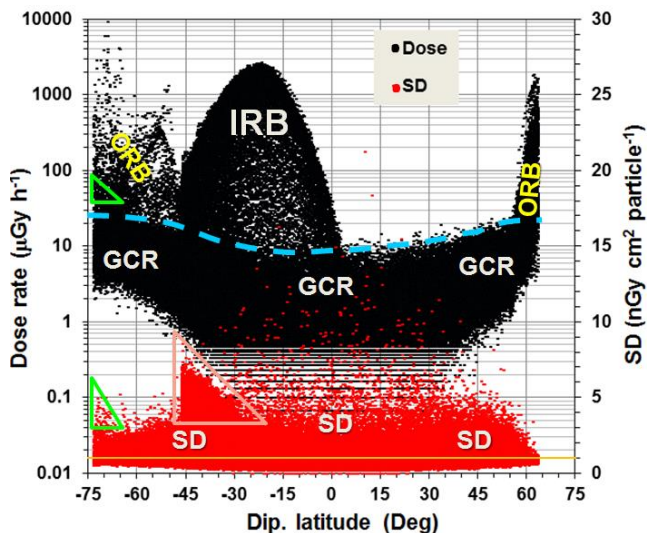

Fig. 2. Presentation of the all R3DR2 data in magnetic dipole coordinates

SD is less than 1 nGy cm^2 $particle^{-1}$ then the expected predominant type of radiation in a 10-s exposition time are electrons in the ORB. When the SD is greater than 1 nGy cm^2 $particle^{-1}$, then the predominant source are protons in the IRB. GCR source contributes to both SD ranges. For the "BION-M" No1 satellite data selection (Dachev et al., 2015c) we extend this procedure adding analysis of total magnetic field strength and flux values. The precise differentiation

Table 1. Statistical analysis of the radiation sources obtained with the RDBR2 instrument in the period 23/10-25/11 2014

Source	Number of 10-s meas. [No]/ Duration in days	Hourly av. dose rate min./av./max. [μGy h⁻¹] Daily av. dose rate min./av./max. [μGy d⁻¹]	Obs. dose rate min./max. [μGy h⁻¹] Obs. flux min./max [cm⁻² s⁻¹]	Total dose rate [mGy] Fluence [No of events/ particles]	Aver. Alt. [km]	Aver. Lat. [Deg.] Aver. L Value	Aver. Long. [Deg.]	Dose rate [μGy h⁻¹] Flux [cm⁻² s⁻¹]	SD [nGy cm² part⁻¹]/ B [Gauss]/ L
All data	285,418 33.03	Hourly aver.=30.16 Daily aver.=724	0.4/10,506 0.26/4,315	23.913 24,582,180	420	-0.05° 1.83	0.044°	No	No
GCR	249,717 28.9	**R3DR=2.841/3.392/ 3.737** R3DR2=2.969/3.143/ 3.413 **R3DR=68.18/81.4/ 89.69** R3DR2=71.26/75.43 81.91	0.033/29.6 0.34/6.95	2.19 4,078,000	419.5	3.38° 1.8	3.1°	Flux<7	B>0.23
IRB (SAA)	17,018 1.97	**R3DR=239/343/431** R3DR2=322/371/431 **R3DR=326/506/713** R3DR2=518/598/704	20/2,670 0.6/295	19.36 14,141,360	424	-32.4° 1.64	-34.7°	Dose>20	SD>1.12
ORB	5,018 0.58	**R3DR=18/110/1562** R3DR2=20/106/330 **R3DR=0.64/89/2348** R3DR2=0.1/63/235	16/10,506 7/4,315	2.1 5,961,520	425	0.5° 4.33°	0.71°	Flux>7	SD<0.8
SEP	50 0.0058	57.2	40/84.6 2.6/10.8	0.0081 5,440	431	-51° 5.4	116°	D>40 Lat.<0°	SD>1.12 B>0.26

of the CGR source in the dose rate interval of values between 5 and 30 µGy h^{-1} from IRB and ORB source continues to be problematic because even the deposited energy spectra are looking very similar.

For the hourly and daily averaged data of R3DE instrument we developed another similar data selection procedure, described comprehensively in Dachev et al. (2012a). This procedure was used historically for data selection of the R3DR instrument on the EXPOSE-R mission (Dachev et al., 2015a). For the purposes of continuity here we will continue to use, for the hourly and daily averaged data (column 3 of Table 1), the procedure described by Dachev et al. (2012a), while for other average data selections and calculations we use the procedure developed by Dachev et al. (2015c). Both procedures are giving very similar averaged results.

The absorbed dose rates and specific doses obtained by the RDR2 instrument during the whole monitoring period (from 23 October to 25 November 2014) are plotted in Fig. 2. The black points against the left axis in the upper part of the figure correspond to the observed dose rates in µGy h^{-1}. The specific dose (SD) variations calculated from the dose rate to flux ratio in nGy cm^2 particle^{-1} (Heffner, 1971, Dachev, 2009, Dachev, 2013b) are plotted in red color against the right axis in the lower part of the figure. On the horizontal axis we choose the geomagnetic dipole latitude (Fraser-Smith, 1987), which, similar to the L value (McIlwain, 1961), organizes well the geomagnetic dependent parameters of the space radiation but allows understanding the differences in both geomagnetic hemispheres. The dark yellow line in the bottom of the Fig. 2 shows the position of the SD value equal to 1.

The heavy, light blue, dashed curve in the center of Fig. 2 is drawn for better understanding the contribution of the different radiation sources. The GCR source is distributed below the curve, while the IRB trapped protons source in the region of the SAA and ORB relativistic electrons source are plotted above the curve. Fig. 2 shows the whole dynamics of the observed dose rates over 8 orders of magnitude. The smallest GCR dose rate values of about 0.033 µGy h^{-1} are situated close to the geomagnetic equator, while the largest obtained are in the Southern Hemisphere ORB region where they reach 10,000 µGy h^{-1}.

The large maximum situated in the Southern Hemisphere of Fig. 2 reaching about 2500 µGy h^{-1} were obtained during the ISS crossings of the SAA region where the inner radiation belt, populated with high-energy protons is encountered. The IRB comes at the ISS altitudes due to a displacement of the magnetic dipole axes from the Earth's center. The maxima in the high latitude regions of both hemispheres are obtained during the crossings of the ORB source. Their poleward boundaries are at different latitudes (65°N in the Northern and 75°S in Southern Hemisphere) because of the asymmetry in the Earth's magnetic field. The poleward boundaries seen as vertical lines are generated in the dipole latitude coordinate system when the station reaches its maximal magnetic elongation and starts to return back to the magnetic equator.

The analysis of the specific dose variations (lower part of Fig. 2) shows the following: (i) the specific doses corresponding to the points of the GCR source, close to the geomagnetic equator, are distributed in the whole range between 0.187 and 22 nGy cm^2 particle^{-1}. This is explained with the large variations of the dose rates being dependent of the deposited energy from the very low amount of particles; (ii) at higher latitudes the relative deviation of GCR source is smaller with a tendency of all data to be close to 1 nGy cm^2 particle^{-1}; (iii) the data separated in the pink triangle in the Southern Hemisphere correspond to the South-Eastern part of the SAA. The calculated SD values there are relatively large, reaching values of 7−8 nGy cm^2 particle^{-1}. This is explained with relatively low proton energies there, which will be further studied in Fig. 8 of this paper; (iv) the SD data separated in the green triangle in the region above 65°S dipole latitude shows unexpected large SD values between 1 and 5 nGy cm^2 particle^{-1}, which suggests the existence of a source different from ORB, the SD values of which are smaller than 1 nGy cm^2 particle^{-1}. We explain this with the observation of proton fluxes in the SEP in the 1-2 November time period. An analog green triangle is drawn in the dose rate data but because the contamination by ORB dose rates the SEP contribution is not clearly seen.

In Table 1 are summarized the observations for the different radiation sources, presented on Fig. 2, and is provided statistics of the measured values. All b text refers to the R3DR2 data. The limited amount of bold text (in the third column) was obtained during R3DR mission in 2009−2010. Here the R3DR data are presented for comparison with the R3DR2 data. The data in column 3 of Table 1 are selected using the selecting procedure published in (Dachev et al., 2012). The selecting requirements presented in the last 2 columns of Table 1 are valid for the selection of all other columns of Table 1.

The number of measurements, the hourly and daily average, and total accumulated dose rates, and fluences are calculated and presented for all data and for each of the four major sources. The averaged coordinates: longitude, latitude, L value and altitude where the averaged values are obtained, are also presented in 3 columns. The presented values in the "All data" row of the table cover all data collected in the period 23 October − 25 November 2014.

GCR radiation source data were selected using two requirements: (i) The flux values to be less than 7 cm^{-2} s^{-1}, which cuts the high flux level in the ORB (cf. Fig. 2); (ii) The total magnetic field strength to be greater than 0.23 Gauss, which cuts the data obtained inside the SAA region (cf. Fig. 7c) where only the isoline with a total magnetic field strength of 0.23 Gauss is presented with a heavy dashed line). The average daily value was obtained by averaging all observed GCR single measurements for each full day. The data of 31 full days are used.

The IRB (SAA) radiation source data in Table 1 were selected also by two requirements. The first is that the dose rate values have to be higher than 20 μGy h^{-1}. This cuts the GCR dose rates, which usually deposited smaller values.

The second requirement is the SD value has to be higher than 1.12 nGy cm^2 particle^{-1}. According to Heffner's formulae (Heffner, 1971) this selects only depositions by protons excluding relativistic electrons and/or *bremsstrahlung* dose rates higher than 20 μGy h^{-1}. The IRB data covered 31 full days.

The ORB radiation source data in Table 1 were selected by: (i) the flux values to be higher than 7 cm^{-2} s^{-1}, which cuts the low flux level in the GCR; (ii) the SD value to be less than 0.8 nGy cm^2 particle^{-1}. According to Heffner's formulae (Heffner, 1971) this selects only depositions by relativistic electrons and/or *bremsstrahlung* excluding proton depositions from GCR or IRB.

The SEP radiation source data in Table 1 were selected by: (i) only data from 1 and 2 November 2014; (ii) in the Southern Hemisphere because here the ISS reached higher L values; (iii) dose rates to be higher than 40 μGy h^{-1} which excludes any GCR contaminations; (iv) SD values to be higher than 1.12 nGy cm^2 particle^{-1} excluding ORB contamination.

The comparison of the averaged values obtained with the R3DR2 instrument in October−November 2014 with analog R3DR values obtained in the March 2009−August 2010 time interval reveals the following results: (i) the GCR average daily dose rate of 75.43 μGy day^{-1} obtained during the EXPOSE-R2 mission is lower than that measured on the EXPOSE-R mission (Dachev et al., 2015a) of 81.4 μGy d^{-1} because a larger part of the EXPOSE-R mission was performed in the time of lower solar activity and respectively higher GCR flux. The higher EXPOSE-R2 mission orbit of about 420 km in comparison with the 360 km orbit of EXPOSE-R mission does not play an important role because of small GCR altitudinal dependence.

Comparison of R3DR2 L>4 GCR flux data with Oulu NM counts rate data

Our first concern, starting to analyze the R3DR2 GCR data, was how well the data obtained in October−November 2014 follow the tendency of the GCR flux decrease in dependence of the solar activity increase of the 24th cycle. One possible way to answer this question was to compare the GCR "free space" data obtained by the RADOM instrument on the Chandrayaan-1 satellite in 2008 (Dachev et al., 2011a) with the new 2014 R3DR2 GCR data obtained at L values bigger than 4 (McIlwain, 1961; Heynderickx et al., 1996). We choose a L>4 value because the knee in the GCR L-profile is at L=3.5 (Dachev et al., 2012a) and we may expect that all GCR radiation exposure values above L=4 are obtained in the open Earth magnetic field lines, i.e. in conditions very close to the free space. Also these GCR radiation environment data to be compared with the Oulu Neutron Monitor (NM) station count rates (http://cosmicrays.oulu.fi/).

Table 2. Comparison of data obtained by R3DR2 and RADOM instrument with Oulu NM data

RADOM data (GCR, "free space")			R3DR2 data (GCR, L>4)			Oulu NM data		Ratio flux R3DR2/RADOM	Ratio dose rate R3DR2/RADOM	Ratio Oulu 2008/2014
Date/ No of meas.	Av. dose rate [µGy h⁻¹]	Av. flux [cm⁻² s⁻¹]	Date/ No of meas.	Av. dose rate [µGy h⁻¹]	Av. flux [cm⁻² s⁻¹]	Av. counts 20 Oct.-20 Nov. 2008	Av. counts 23 Oct.-25 Nov. 2014			
04-08 Nov. 2008/ 33,000	12.76	3.14	23 Oct.- 25 Nov. 2014/ 7,438	10.33	2.75	6713	6129	0.876	0.81	0.913

Table 3. Spectra explanation

Spectra name	Number of primary spectra	Av. dose rate (µGy h⁻¹)	Av. orbit coordinates and selecting requirements					
			Date	Lat./Long. (Deg.)	Alt. (km)	Dose rate (µGy h⁻¹)/ Ener. (MeV)	L value/ B (Gauss)	SD (nGy cm² part.⁻¹) Flux (cm⁻² s⁻¹)
GCR; L>4	5687	9.42	23/10-25/11/2014		430	D<20	L>4	
SEP, 2014	50	54.2	01-02/11/2014	Lat. <0°	431	D>20	L>4	
ORB	5,018	146.1	23/10-25/11/2014	0.5°/0.71°	425	Flux>7		SD<0.8
IRB	17,018	370.7	23/10-25/11/2014	-32.4°/-34.7°	424	D>20		SD>1.12
GCR	249,717	3.16	23/10-25/11/2014	Lat. <0°	430		B>0.23	Flux<7
GCR; E-E	More than 2,500,000	3.63	03/2008-09/2009	All/All	365			
IRB; D=45	284	45	23/10-25/11/2014	-40°/-5°	428	D~45; E~11		
SEP, 2001	66 from MDU-2&3	12.1	20/05/2001				L>5	

In Table 2 is summarized the available information and it is seen that the obtained average flux ratio between R3DR2 and RADOM data in 2014 and 2008 (0.876) coincide relatively well with the Oulu NM count rate ratio (0.913) for similar periods in same years. The dose-rate ratio of 0.81 is not so close to the flux ratio but this can be expected for a stochastic process, which the dose deposition is.
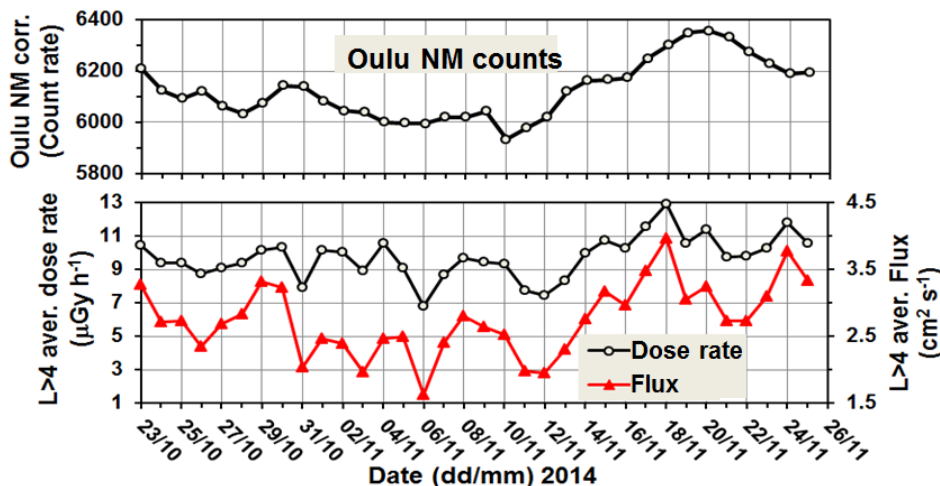

Fig. 3. Comparison between the daily averaged R3DR2 L>4 flux and dose rate data (lower panel) with the Oulu Neutron Monitor (NM) count rates data (upper panel)

On Figure 3 is presented a comparison between the R3DR2 L>4 daily average flux and dose-rate data (lower panel) with the Oulu NM count rates data (upper panel) for the period 23 October−25 November. It could be seen that during the flight of the EXPOSE-R2, in October−November 2014, the averaged flux data per day varied in the interval of 1.5-3.75 cm^{-2} s^{-1}, while the dose rate varied in the interval of 7-13 µGy h^{-1}. The flux and dose rate variations are similar because according to formulae (1) they are in linear dependence. The R3DR2 flux and dose rate curves follow relatively well the Oulu NM curve, which give us the information that the L>4 data obtained by the R3DR2 GCR are representative.

ORB daily variations. Comparison with GOES-15 data and planetary Ap index

Relativistic electrons enhancements (REP) in the outer radiation belt are one of the major manifestations of space weather (Zheng et al., 2006; Wren, 2009; Zhao and Li, 2013) in low Earth orbit (LEO). We keep already long time experience in the REP observations on LEO satellites – Foton M2/M3 and ISS (Dachev et al., 2009, 2012b, 2013a). Our active REP observations in the ISS radiation environment were and are still unique (Dachev et al., 2009).
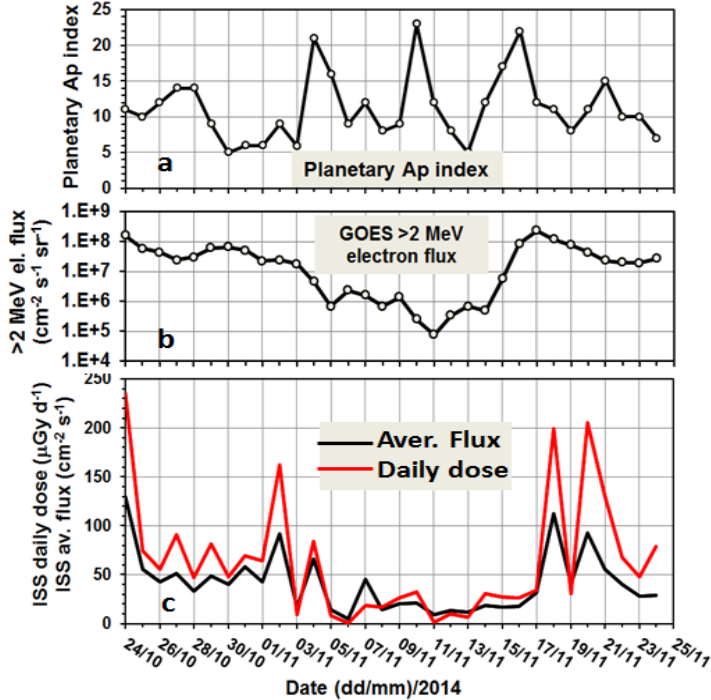
Fig. 4. Daily variations of the ORB dose rates and fluxes (panel "c") observed by R3DR2 instrument. They are compared with GOES-15 >2 MeV electron fluxes in panel "b" and planetary Ap index in panel "a".

The new ISS data in October-November 2014 also contain 5,961,520 counts by relativistic electrons (for more details look at the ORB row in Table 1). In panel "c" of Fig. 4 the daily variations of the ORB relativistic electron dose rates and fluxes observed by R3DR2 instrument are presented. They are compared with GOES-15 >2 MeV electron flux in panel "b" and planetary *Ap* index in panel "a". The *Ap* index is defined as the earliest occurring maximum value for 24 h obtained by computing an eight-point running average of successive three-hour *Ap* indices during a geomagnetic storm event and is uniquely associated with the storm event (http://www.ngdc.noaa.gov/stp/geomag/kp_ap.html). All 3 panels are plotted against the time (date) between 24 October and 24 November 2014.

As it was already noted, the geomagnetic field during the period of the ISS flight in October-November 2014 was at moderate levels with two "strong" and one "moderate" (http://www.swpc.noaa.gov/noaa-scales-explanation) geomagnetic storms on 4, 10 and 16 of November 2014. On Fig. 3 these storms are seen with maxima of the planetary *Ap* index reaching values of 21, 23 and 22 in the central part of panel "a" (ftp://ftp.swpc.noaa.gov/pub/warehouse/2014).

According to our earlier experience with the analysis of the ORB daily variations on the EXPOSE-R mission (Dachev et al., 2015a; see Fig. 6) we expected to observe remarkable enhancements of the ORB daily flux and dose rate after each of the magnetic storm enhancements of the *Ap* index. Unfortunately the first two magnetic storms did not produce any remarkable maxima in both R3DR2 and GOES 15 data. Only the third magnetic storm on 16 November 2014 produced a maxima of the average flux and daily dose rates of >2 MeV electron flux measured by the R3DR2 instrument and GOES-15.

We have to underline that the general trends in the time profiles, obtained on ISS and GOES 15 flux data, match relatively well. The maxima of the relativistic electron flux were observed in the periods 24 October−5 November and 15−24 November, while the minimum was in the period 5−15 November 2014.

The ISS relativistic electron flux maximum on 18 November 2014 in Fig. 4 was delayed by one day in comparison with the >2 MeV flux data from GOES-15 and by two days in comparison with the *Ap* maximum. This is understandable, keeping in mind that there is necessary time for fulfilling of the whole magnetic field line (Zhao and Li, 2013). Our previous experience with the analysis of the R3DR instrument REP data in 2010 (Dachev et al., 2013; see Fig. 5); shows also delay of 2 days between *Ap* maximum on 5 April 2010 and the relativistic electrons flux maximum on 7 April 2010.

The existence of large relativistic electron fluxes in the external radiation environment of the ISS during the October−November 2014 time period, once again confirms our previous findings that this radiation source permanently affects the ISS. That is why it is necessary to keep permanent measurements of the ORB dose rates and especially on the space suit during the ExtraVehicular Activity (EVA) of cosmonauts and astronauts. Under request from our colleagues from Institute of bio-medical problems of the Russian Academy of Science (RAS) we are developing a new Liulin-ISS-2 system (Dachev et al., 2015b), which will perform active measurements on the space suit of the Russian cosmonauts during EVA.

SEP data presentation

Small SEP event was observed in the period 1-7 November 2014. In panel "a" of Fig. 5 are presented the measured proton fluxes by the GOES 15 "Space Environment Monitor (SEM)" with energies >5, >10, and >30 MeV (http://goes.gsfc.nasa.gov/text/databook/section05.pdf). From panel "a" it is seen that the SEP began at about 13:00 UT on 1 November 2014. The maximum in the >30 MeV channel occurred on 3 November 2014 at about 22:00 UTC. The end was on 7 November 2014. No real enhancement in the GOES-15 proton flux with energies >100 MeV was observed (ftp://ftp.swpc.noaa.gov/pub/warehouse/2014).
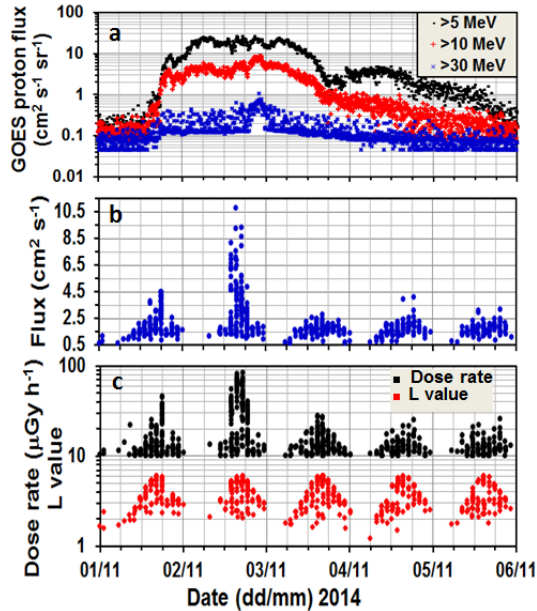
Fig. 5. Presentations of different spectra shapes obtained by the R3DR2 instrument in October−November 2014. (Table 2 presents detailed information for the different curves.)

On Fig. 5 panels "b" and "c" show the dose rates and fluxes measured by the R3DR2 instrument for the same period as the GOES-15 data. In panel "c" except the dose rate in the lower part is presented the L value at which the measurements was made. Data for the panels "b" and "c" were separated under the requirements presented in the last row of Table 1 but dose rates to be more than 10 μGy h^{-1}. We choose this higher dose rate just to show the dynamics of the variations, keeping in mind that only the data with dose rates D>40 μGy h^{-1} undoubtedly belong to the SEP data.

Panels "b" and "c" of Fig. 5 represent the maxima generated when the ISS crosses the Southern Hemisphere from small L values across the maximum of about 6 and back to smaller L values. The main amount of data <20 μGy h^{-1} belongs to the GCR source. The data in the interval 20−40 μGy h^{-1} contains mixed radiation by GCR, ORB, and SPE sources. The SEP data with dose rates D>40 μGy h^{-1} continue to be contaminated by ORB data and this is clearly seen in Fig. 6. We do not have an available procedure to separate them mainly because this is the nature of the radiation sources at these latitudes.

Analysis of the different spectra shapes of the radiation sources

On Fig. 6 are depicted different shapes of the energy deposited spectra obtained mainly by the R3DR2 instrument in October−November 2014. Only the spectra named "SEP, 2001"and "GCR; E-E" were obtained during the DOSMAP

and EXPOSE-E missions in 2001 and 2008-2009, respectively. The "SEP 2001" spectrum is presented to show that in the case of very low dose rates (12.1 μGy h^{-1}) the SEP spectrum shape is similar to the "GCR; L>4" spectrum form.
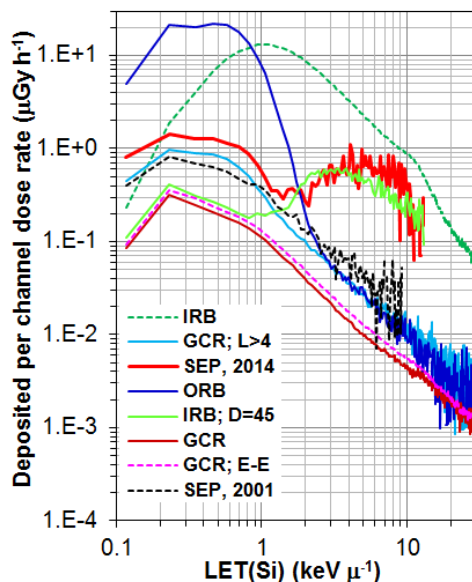

Fig. 6. Presentation of different spectra shapes obtained by the R3DR2 instrument in October−November 2014. (See Table 2 for more detailed information.)

The "GCR; E-E" spectrum is presented to confirm that the EXPOSE-R2 "GCR" spectrum has the same form but lies below the "GCR; E-E" because the solar activity in 2014 was larger than in 2008−2009 and respectively the GCR flux is smaller.

Table 3 contains detailed information for the different spectra in Fig. 6. The individual spectra seen in Fig. 6 are obtained after averaging of various numbers of primary spectra (see column 2 of Table 3.) and are plotted in coordinates of Linear Energy Transfer (LET) in silicon (Si) (keV), per micron/deposited per channel dose rate. This allows a better understanding of the process of formation of the spectra and estimation of the deposited dose rates in the different deposited energy ranges (Dachev, 2009). The deposited dose rate, according to formulae (1), is the area between the abscissa and the curve of the deposited energy spectrum. The "GCR", "IRB", and "ORB" spectra are shown in Fig. 6 only to confirm the spectra shapes described by Dachev (2009) that is why we will not further analyze them.

According to our current understanding the "GCR" and "GCR; E-E" spectra averaged over all latitudes are with quasy-linear falling shape in the coordinates deposited energy/deposited per channel dose rate. A more detailed look

on the shape shows 2 maxima. The first one is at about 0.9−1 keV μ⁻¹, while the second one is at about 11−12 keV μ⁻¹. This form of the spectra can be interpreted as superposition of 3 single maxima generated by H, He and heavier ions (Ca and O) (Dachev et al., 2013c; Zeitlin, 2014).

Most-interesting and new for us is the spectrum seen in the middle of the figure (Fig. 6) named "SEP; 2014". To explain the different parts of "SEP; 2014" spectrum we add 2 well known and expected spectra. First one is named "GCR; L>4". Its shape in the range 0.1−1.5 keV μ−¹ deposited energy is similar to the shape of the spectrum named "ORB" and this is reasonable because: (i) the nature of the radiation at these latitudes; (ii) problems, which we have, with the precise differentiation of the GCR and ORB sources in low dose range 5−30 μ☐Gy h⁻¹. Further the shape of the "GCR, L>4" spectrum is similar to the two "GCR" and "GCR; E-E" spectra but elevated on the abscissa because of higher dose rates observed at higher latitudes, where the lower geomagnetic vertical cutoff rigidity (Shea and Smart, 2001) allows penetrating in the Earth magnetic field higher primary GCR fluxes. Secondly, an additional spectrum, which is the specially selected "IRB; D=45" spectrum with deposited dose rate and mean energy close to the "SEP; 2014" dose and energy (see Table 3). The low energy deposition part of this spectrum is similar to the "GCR" and "GCR; E-E" spectra, while the high energy part is similar to the "IRB" spectrum, which is generated mainly by protons.

The shape of the "SEP; 2014" spectrum is reasonable because: (i) the low energy deposition part of it is similar to the "GCR; L>4" spectrum because at these deposited energies a mixed radiation of GCR and ORB particles is observed. Also the "SEP; 2014" spectrum is collected at the same high latitudes as the "GCR; L>4" spectrum; (ii) the high energy deposition part of this spectrum is similar to the "IRB; D=45" spectrum, which present low energy protons in the South-East part of the SAA.

Global distributions of the dose rate and flux data

Figures 7b and 7c present the averaged contour view of the R3DR2 flux and dose rate global distribution obtained outside the ISS in the period 23−30 October 2014 with 10-s resolutions. In Figure 7a they are compared with the predicted proton fluxes above 100 MeV and electron fluxes above 4 MeV at an altitude of 420 km by the AP/AE-8 MAX models (http://www.spenvis.oma.be/); Vette, 1991).

In Figure 7b, except the world map of the flux, the isolines of the L value (McIlwain, 1961; Heynderickx et al., 1996) for the 2015 epoch at the altitude of the ISS are also presented with dashed magenta lines for L values 1.7 and 2.1. The L=4 isoline is presented with a heavy line. It is seen that the lines of equal fluxes in the north and south high latitude regions follow well the L-shell isolines as expected.

In Figure 7c, except the global map of the dose rate, the isoline of 0.23 Gauss of the total Earth magnetic field strength B for the 2015 epoch at the altitude of the ISS are also presented with a dashed black line. It is seen that this line

32

separates well the area of the SAA, populated with IRB protons with energies between 30−500 MeV from the GCR region around it.

On Figure 7b and 7c the areas outside the SAA region present the averaged GCR flux and dose rate distribution, forming a wide minimum close to the magnetic equator and rise toward the higher latitudes in both hemispheres.
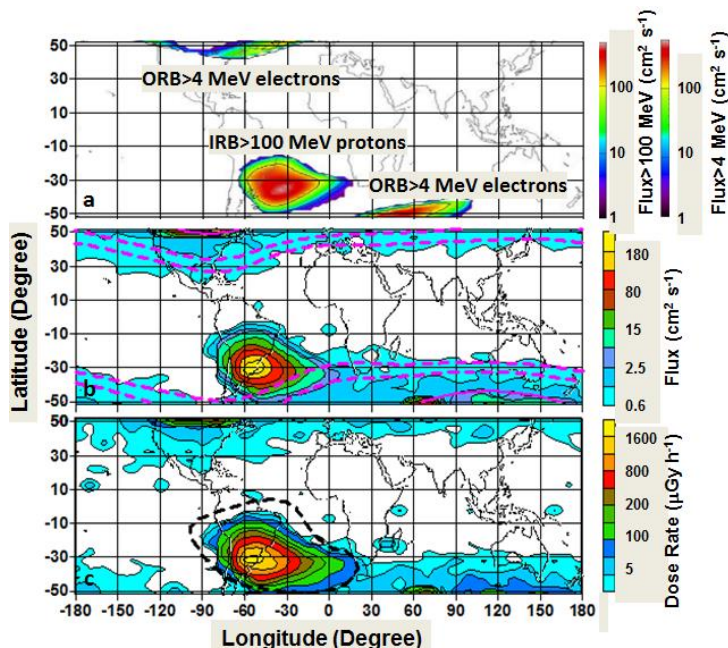

Fig. 7. Figures 7b and 7c present the global distribution of the R3DR2 flux and dose rate data for the period 23−30 October 2014, which are compared with the predicted ones by the AP-8/AE-8 MAX models proton fluxes above 100 MeV and electron fluxes above 5 MeV in Figure 3a.

The observed flux maximum at L=4.4 shows the position and shape of the ORB maximum, which is distributed wider in longitude than the AE8 MAX predictions. The absolute maxima of the R3DR2 ORB data are at latitudes above 45° in both hemispheres. Their coordinates in longitude are 70 °E in the Southern Hemisphere and 80 °W in the Northern Hemisphere. These coordinates coincide well with the AE8 MAX predictions. The comparison of the averaged flux values inside the ORB maxima shows that the predicted model values are in the range 150−300 cm^{-2} s^{-1}, while the measured ones are 140 cm^{-2} s^{-1} in the Southern Hemisphere and 193 cm^{-2} s^{-1} in the Northern Hemisphere.

Recent electron flux data in the 0.5−0.6 MeV and 0.8−1.0 MeV energy range, measured by the energetic particle telescope (EPT) from 29 May 2013 to 20 August 2013 onboard the PROBA-V spacecraft (Cyamukungu et al., 2014; Pierrard et al., 2014) shows well seen global maxima in both hemispheres with a

tendency that the Sothern Hemisphere maximum is separated at two parts for the higher energy. The position of the largest electron flux in the 0.8−1.0 MeV energy range of EPT data coincide well with the absolute R3DR2 maximum with coordinates 45°E−80°E, 47°S−50°S (http://space-env.esa.int/index.php/esa-estec-space-environment-tec-ees/articles/EPT_first_results.html). The ORB maximum observed by EPT in the high Northern latitudes also coincides well with our data.

The external oval of the SAA R3DR2 data in Fig. 7b and the one predicted by the AP-8 MAX model in Fig. 7a are very similar and this verifies well our data. We average the coordinates of 373 measurements of the absorbed dose with values more than 2000 μGy h^{-1} and obtain that the R3DR2 SAA maximum is situated at (50.5°W, 31.2°S) at an average altitude of 421 km. 547 measurements of the more than 200 cm^{-2} s^{-1} flux rate gives the average SAA maximum flux coordinates at (51.9°W, 30.0°S). The SAA maximum occurs mainly at the ascending orbits. Only 17 dose rate points of 373 were found at descending orbits. This is in accordance with our previous findings (Dachev et al., 2011b). The explanation is that the R3DR2 instrument is mounted on the left-hand side of *Zvezda* module, against the ISS vector velocity is situated to receive larger amounts of westward drifting protons in the maximum of the SAA on the ascending orbits when the ISS is in the usual XVV attitude (http://spaceflight.nasa.gov/station/flash/iss_attitude.html).

The geographic coordinates of the SAA maximum are influenced by the secular drift of the geomagnetic field (Fraser-Smith, 1987), which leads to a movement of the SAA maximum in the North-West direction. The calculated yearly rate of the SAA flux maximum westward secular drift (Wilson et al., 2006) is 0.3° per year, that is why the calculated 2014 position is 44 (years)*0.3°=13.2° than the calculated SAA flux maximum position is at 48.2°W, which is by 3.7° less than measured with the R3DR2 flux maximum position. The drift rate calculated by us is 0.384° per year, which is in good agreement of the average value of 0.45° per year obtained for the minimum of the solar activity (Qin at al., 2014).

The EPT (Cyamukungu et al., 2014; Pierrard et al., 2014) SAA 90-126 MeV maximum at 820 km altitude can be visually estimated to be at coordinates (55°W, 25°S), which is even more westward than our result. The smaller southward latitude of the SAA maximum in PROBA-V spacecraft data is reasonable because these data are obtained at altitudes around 800 km (Ginet et al., 2008). Qin at al., (2014) also reported that the longitudinal position of the SAA maximum was at 53°W in 2010 for >16 MeV proton flux data obtained with an upgraded version of the Space Environment Monitor (SEM 2) (Evans and Greer, 2000) at 800 km altitude by the NOAA-15 satellite.

Global distributions of the specific dose (SD) data

Figure 8b presents the global distribution of the SD data, which was previously shown in the pink triangle in Fig. 2. The black heavy dashed line presents the isoline of 0.23 Gauss of the total Earth magnetic field strength, which separates the SAA region. It is seen that the calculated SD values in the North-West part of the SAA have values of 1.12 to 2 nGy cm^2 particle^{-1}, which according to the Heffner's formula (Heffner, 1971; Dachev, 2009) correspond to proton energy in the range of 200−47 MeV. In the South-East part of the SAA region a well-defined maximum is formed. The average SD value in the maximum is 4.8 nGy cm^2 particle^{-1}, which correspond to proton energy at the detector of
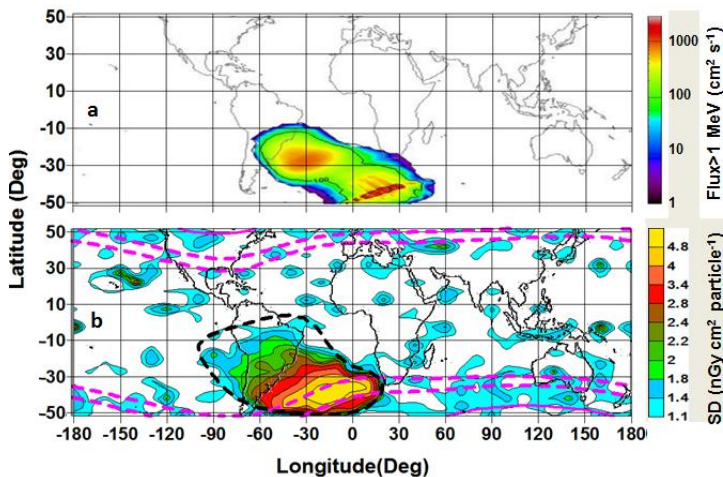
Fig. 8b presents the global distribution of the R3DR2 dose rate to the flux ratio or the specific dose. Data are compared with the world map of the 1 MeV energy proton flux predicted by the AP8 MAX model at 420 km altitude in Fig. 8a.

13.8 MeV. We suppose that the R3DR2 maximum in SD is formed because of a local maximum in the low energy proton flux, that is why we try to find a confirmation of this idea, preparing Fig. 8a, which presents the proton fluxes above 1.0 MeV energy predicted by AP8 MAX (http://www.spenvis.oma.be/); (Vette, 1991). In contrast to the usual higher energies SAA maximum, two separated maxima are seen: (i) at 5° eastward from the regular position of the SAA and (ii) in the South-Eastern part of it, which extends in the range 0°E−30°E longitude. The form of the AP8 MAX maximum is similar to the form of the R3DR2 maximum in SD, but it is about 30° more towards East than the position of the maximum in Fig. 8b.

The centrum of the AP8 MAX 1 MeV maximum in the South-East part of the SAA region in 1970 can be estimated at (15°E, 43°S). The calculated yearly rate of the SAA maximum westward drift is 0.3° per year (Wilson et al., 2006).

Then the calculated position for 2014 in longitude is 44 (years)*0.3°=13.2°. In total, this is giving 15°-13.2°=1.8°, which is about 18° less than necessary to coincide with the R3DR2 maximum in SD. The reported by cellular westward drift rate is dependent by the solar activity (Qin at al., 2014).

On the other hand the geographic distribution of the protons with energies 1−5 MeV measured by the Coronas-F satellite in 2001 show the second maximum at coordinates (6°E, 48°S), which is much closer to the center of the SD maximum in Fig. 8b at (13°W, 38°S) (Kuznetsov et al., 2008; 2010).

On Fig. 9 are presented the longitudinal profiles of the flux, SD and proton energy at the surface of the detector R3DR2 for the latitude range between 35°S and 30°S. To avoid bifurcation of the data only the ascending orbits data are presented. The two trendlines of SD and energy are calculated for six orders polynoms. They are shown only with an illustrative purpose; that is why we do not present the formulas of the polynoms.
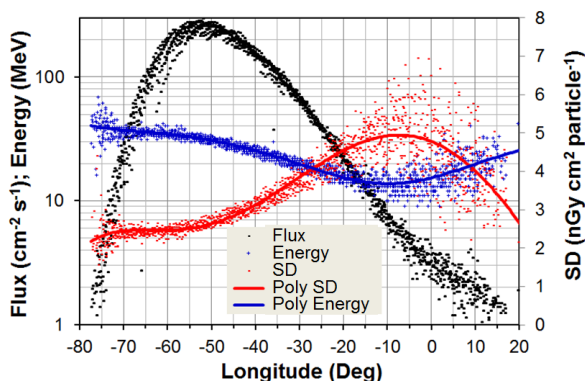

Fig. 9. Longitudinal profiles of the flux, SD, and proton energy for the latitude range between 35°S and 30°S.

It is seen that the absolute flux maximum is at about 52°W longitude where the position of the SAA maximum is. A secondary not very well formed proton flux maximum is seen in the longitude range of about 10°W−10°E. In the same range the maximum of SD is formed and the minimum of the calculated proton energy, respectively.

The proton energy at the surface of the detector is calculated from the SD value using the Heffner formula (Heffner, 1971; Dachev, 2009). The average SD value for the whole Fig. 9 of 3.6 nGy cm^2 particle^{-1} corresponds to 24 MeV protons energy at the surface of the detector. The smallest value of SD of 1.57 nGy cm^2 particle^{-1} corresponds to protons with energy of 69 MeV. The largest SD value, seen in Fig. 9 of 7 nGy cm^2 particle^{-1} corresponds to 9 MeV protons energy at the surface of the detector.

Conclusions

This article analyses the results for the ISS radiation environment obtained by the R3DR2 instrument inside the EXPOSE-R2 facility, generated by different radiation sources, including: galactic cosmic rays (GCRs), inner radiation belt (IRB) trapped protons in the region of the South Atlantic Anomaly (SAA), outer radiation belt (ORB) relativistic electrons, and Solar Energetic Protons (SEP). The first month (24 October−25 November 2014) of the EXPOSE-R2 active data collection mission is covered.

The comparison of the values obtained with the R3DR2 instrument in October−November 2014 with analog R3DR values in the period of 2009−2010 reveal the following results: (i) the GCR average daily dose rate obtained during the EXPOSE-R2 mission is lower than that measured one on the EXPOSE-R mission (Dachev et al., 2015c) because a larger part of the EXPOSE-R mission was performed in the time of lower solar activity and higher GCR flux, respectively; (ii) the IRB average daily dose rate of 598 μGy d^{-1} obtained during the EXPOSE-R2 mission is higher than that measured during the EXPOSE-R mission (Dachev et al., 2015c) of 506 μGy d^{-1} because the EXPOSE-R2 mission orbit was about 60 km higher than the EXPOSE-R mission (360 km); (iii) the ORB average daily dose rate of 63 μGy day^{-1} obtained during the EXPOSE-R2 mission is lower than that measured during the EXPOSE-R mission (Dachev et al., 2015c) of 89 μGy d^{-1} because the EXPOSE-R mission took place during the second largest relativistic electrons precipitation (REP) event in GOES history in the period 7 April−7 May 2010 (Dachev et al., 2013a), when the highest observed values of 2,347 mGy d^{-1} occurred in the R3DR data on 7 April 2010.

For the first time in the history of using of the Liulin-type energy deposition spectrometers (Dachev et al., 2015b) a flux from solar energetic particles (SEP) in the period 1−4 November 2014 were detected; (3) the SEP energy deposition spectra were compared with other well-known spectra and confirmed the SEP spectra shape.

The dynamics of the ORB doses measured for the first month of the EXPOSE-R2-mission periods confirm conclusions made by Dachev et al. (2013) that the ORB relativistic electrons are common on the ISS. Although the obtained doses do not pose extreme risks for the astronauts being on EVA, they have to be considered as a permanently present source, which requires additional comprehensive investigations.

References

1. Badavi, F.F., 2014. Validation of the New Trapped Environment AE9/AP9/SPM at Low Earth Orbit, Advances in Space Research, 54, 917-928. http://dx.doi.org/10.1016/j.asr.2014.05.010.
2. Bartels, J., Heck, N.H. & Johnston, H.F., 1939. The three-hour range index measuring geomagnetic activity. Geophys. Res., 44, 411-454.
3. Berger, M.J., Coursey, J.S., Zucker, M.A., Chang, J. Stopping-power and range tables for electrons, protons, and helium ions. NIST Standard Reference Database 124, Available online at: http://www.nist.gov/pml/data/star/index.cfm, October, 2013.
4. Berger, T., Hajek, M., Bilsk, P., Körner C., Vanhavere F., Reitz G. 2012, Cosmic radiation exposure of biological test systems during the EXPOSE-E mission, Journal of Astrobilogy, 12(5), 387-392. DOI: 10.1089/ast.2011.0777.
5. Cyamukungu, M., Benck, S., Borisov, S., Gregoire, G., Cabrera, J., Bonnet, J. L., & Nieminen, P., 2014. The Energetic Particle Telescope (EPT) on board PROBA-V: description of a new science-class instrument for particle detection in space. Nuclear Science, IEEE Transactions on, 61(6), 3667-3681.
6. Cucinotta, F.A., Schimmerling, W., Wilson, J.W., Peterson, L.E., Saganti, P.B., and Dicello. J.F., 2004, Uncertainties in estimates of the risks of late effects from space radiation. Adv. Space Res., 34, 1383–1389.
7. Dachev, T.P., Tomov, B., Matviichuk, Yu., Dimitrov, Pl., Lemaire, J., Gregoire, Gh., Cyamukungu, M., Schmitz, H., Fujitaka, K., Uchihori, Y., Kitamura, H., Reitz, G., Beaujean, R., Petrov, V., Shurshakov, V., Benghin, V., Spurny, F., 2002. Calibration results obtained with Liulin-4 type dosimeters. Advances in Space Research 30, 917–925, http://dx.doi.org/10.1016/S0273-1177(02)00411-8 .
8. Dachev, T.P., 2009. Characterization of near Earth radiation environment by Liulin type instruments. Advances in Space Research, 44, 1441–1449, http://dx.doi.org/10.1016/j.asr.2009.08.007.
9. Dachev, Ts., Tomov, B.T., Matviichuk, Yu.N., Dimitrov, P.G., Bankov, N.G. 2009. Relativistic electrons high doses at international space station and Foton M2/M3 satellites. Adv. Space Res., 44 1433–1440, http://dx.doi.org/10.1016/j.asr.2009.09.023.
10. Dachev, T.P., Semkova, J., Tomov, B., Matviichuk, Yu., Dimitrov, Pl., Koleva, R., Malchev, St., Reitz, G., Horneck, G., De Angelis, G., Häder, D.-P., Petrov, V., Shurshakov, V., Benghin, V., Chernykh, I., Drobyshev, S., and Bankov. N.G., 2011a. Space shuttle drops down the SAA doses on ISS. Adv Space Res. 11:2030–2038, http://dx.doi.org/10.1016/j.asr.2011.01.034.
11. Dachev, T., Angelis, G., Semkova, J., Tomov, B., Matviichuk, Yu., Dimitrov, Pl., Bankov, N., Reitz, G., Horneck, G., Häder, D.-P., 2011b. Further analysis of the space shuttle effects on the ISS SAA doses, paper IAC-11,A1,4,2,x9918, IAF Congress, 2011. http://www.iafastro.net/iac/paper/id/9918/summary.lite/
12. Dachev, T.P., Horneck, G., Häder, D.-P., Lebert, M., Richter, P., Schuster, M., Demets, R., 2012a. Time profile of cosmic radiation exposure during the EXPOSE-emission: the R3D instrument. Journal of Astrobiology 12 (5), 403–411, http://eea.spaceflight.esa.int/attachments/spacestations/ID501800a9c26c2.pdf

13. Dachev, T.P., Tomov, B.T., Matviichuk, Yu.N., Dimitrov, Pl.G., Bankov, N.G., Reitz, G., Horneck, G., Häder, D.-P., Lebert, M., Schuster, M., 2012b. Relativistic electron fluxes and dose rate variations during April–May 2010 geomagnetic disturbances in the R3DR data on ISS. Advances in Space Research 50, 282–292, http://dx.doi.org/10.1016/j.asr.2012.03.028.

14. Dachev T.P., 2013a. Analysis of the space radiation doses obtained simultaneously at 2 different locations outside ISS. Adv. Space Res., 52, 1902-1910, http://dx.doi.org/10.1016/j.asr.2013.08.011

15. Dachev, T.P., 2013b. Profile of the ionizing radiation exposure between the Earth surface and free space. Journal of Atmospheric and Solar-Terrestrial Physics, 102, 148–156, http://dx.doi.org/10.1016/j.jastp.2013.05.015.

16. Dachev, T.P., Ploc, O., Sihver, L., 2013c. Estimation of the dominant ion composition in space using the Liulin and PHITS simulations, Workshop on Radiation Measurements on ISS, Budapest, Hungary, 3-5 September 2013. http://wrmiss.org/workshops/eighteenth/Ploc.pdf

17. Dachev, T.P., G. Horneck, G., D.-P. Häder, D.-P., M. Schuster, M., and M. Lebert, 2015a. EXPOSE-R cosmic radiation time profile, Journal of Astrobilogy, 14, 17-25. http://dx.doi.org/10.1017/S1473550414000093.

18. Dachev, T.P., J.V. Semkova, J.V., Tomov, B.T., Matviichuk, Yu.N., Dimitrov, Pl.G., Maltchev, S., Koleva, R., Bankov, N.G., Shurshakov, V.V. Benghin, V.V., Yarmanova, E.N., Ivanova, O.A. Häder, D.-P., Lebert, M., Schuster, M.T. Reitz, G., Horneck, G., Uchihori, Y., Kitamura, H., Ploc, O., Kubancak, J., Nikolaev, I., 2015b. Overview of the Liulin type instruments for space radiation measurement and their scientific results, Life Sciences in Space Research, 4, 92–114, 2015. http://dx.doi.org/10.1016/j.lssr.2015.01.005

19. Dachev, T.P., Tomov, B.T., Matviichuk, Yu.N., Dimitrov, Pl.G., Bankov, N.G., Shurshakov, V.V., Ivanova, O.A., Häder, D.-P., Schuster, M.T., Reitz, G., Horneck, G., 2015c. "BION-M" No1 spacecraft radiation environment as observed by the RD3-B3 radiometer-dosimeter in April-May 2013, Journal of Atmospheric and Solar-Terrestrial Physics. 123, 82-91, 2015. http://dx.doi.org/10.1016/j.jastp.2014.12.011.

20. Damasso, M., Dachev, Ts., Falzetta, G., Giardi, M.T., Rea, G., Rea, G., Zanini, A., 2009. The radiation environment observed by Liulin-Photo and R3D–B3 spectrum-dosimeters inside and outside Foton-M3 spacecraft. Radiat. Meas. 44 (3), 263–272, http://dx.doi.org/10.1016/j.radmeas.2009.03.007.

21. Evans, D. S., and Greer, M. S., 2000. Polar Orbiting Environmental Satellite Space Environment Monitor-2: Instrument Description and Archive Data, U.S. Dep. of Commer., Natl. Oceanic and Atmos. Admin., Oceanic and Atmos. Res. Lab., Space Environ. Cent., Boulder, Colo.

22. Fraser-Smith, A. C., 1987. Centered and eccentric geomagnetic dipoles and their poles 1600-1985. Rev. Geophys., 25, 1-16.

23. Galperin, Yu.I., Ponamarev, Yu.N., Sinizin, V.M., 1980. Some Algorithms for Calculation of Geophysical Information along the Orbit of Near Earth Satellites. Report No 544. Space Res. Inst., Moscow (in Russian).

24. Ginet, G.P., Madden, D., Dichter, B.K., Brautigam, D.H. Energetic Proton Maps for the South Atlantic Anomaly, AFRL-RV-HA-TR-2008-1060, 2008. http://www.dtic.mil/cgi-bin/GetTRDoc?AD=ADA485155.

25. Heffner, J., Nuclear radiation and safety in space. M, Atomizdat, 115 p., 1971. (in Russian).

26. Heynderickx, D., Lemaire, J., Daly, E. J. 1996, Historical review of the different procedures used to compute the L-Parameter. Rad. Measur. 26, 325-331.

27. Häder, D.-P. and Dachev, T.P., 2003. Measurement of solar and cosmic radiation during spaceflight. Kluwer Press, Surveys in Geophysics, 24, 229-246.

28. Häder, D.-P., Richter, P., Schuster, M., Dachev, Ts., Tomov, B., Dimitrov, P., Matviichuk, Yu., 2009. R3D-B2—Measurement of ionizing and solar radiation in open space in the BIOPAN 5 facility outside the FOTON M2 satellite. Advances in Space Research, 43, 1200–1211, doi: 10.1016/j.asr.2009.01.021.

29. Kuznetsov N.V., Nikolaeva N.I., Panasyuk M.I., Trapped proton fluxes observed by LEO satellites in 23d solar cycle, 2008. WRMISS13Kraków, PolandSeptember8-10, 2008. http://wrmiss.org/workshops/thirteenth/Kuznetsov.pdf

30. Kuznetsov, N. V., Nikolaeva, N. I. and Panasyuk M. I., 2010. Variation of the trapped proton flux in the inner radiation belt of the Earth as a function of solar activity, Cosmic Res., 48(1), 80–85.

31. McIlwain, C. E., 1961. Coordinates for mapping the distribution of magnetically trapped particles. J. Geophys. Res., 66, 3681-3691.

32. Nealy, J.E., Cucinotta, F.A., Wilson, J.W., Badavi, F.F., Zapp, N., Dachev, T., Tomov, B.T., Semones, E., Walker, S.A., Angelis, G.De, Blattnig, S.R., Atwell, W., 2007. Preengineering spaceflight validation of environmental models and the 2005 HZETRN simulation code. Advances in Space Research 40, 1593–1610, doi: 10.1016/j.asr.2006.12.029.

33. Nymmik, R.A., 2007. Improved environment radiation models. Adv. Space Res. 40, 313–320.

34. Pierrard, V., Rosson, G. L., Borremans, K., Lemaire, J., Maes, J., Bonnewijn, S., ... & Nieminen, P., 2014. The Energetic Particle Telescope: First Results. Space Science Reviews, 184(1-4), 87-106.

35. Ploc, O., Spurny, F., Dachev, Ts.P., 2011. Use of energy depositing spectrometer for individual monitoring of aircrew. Radiat. Prot. Dosim.144 (1–4), 611–614. http://dx.doi.org/10.1093/rpd/ncq505.

36. Qin, M., X. Zhang, B. Ni, H. Song, H. Zou, and Y. Sun, 2014. Solar cycle variations of trapped proton flux in the inner radiation belt, J. Geophys. Res. Space Physics, 119, 9658–9669, doi:10.1002/2014JA020300.

37. Rabbow, E., Rettberg, P., Barczyk, S., Bohmeier, M., Parpart, A., Panitz, C., ... & Reitz, G. (2015). The astrobiological mission EXPOSE-R on board of the International Space Station. International Journal of Astrobiology, 14(01), 3-16 doi: 10.1017/S147355041400069X.

38. Reitz, G., Beaujean, R., Benton, E., Burmeister, S., Dachev, T., Deme, S., Luszik-Bhadra, M., Olko, P., 2005. Space radiation measurements on-board ISS-The DOSMAP experiment. Radiation Protection Dosimetry 116 (1–4), 374–379.

39. Slaba, T.C., Blattnig, S.R., Badavi, F.F., Stoffle, N.N., Rutledge, R.D., Lee, K.T., Zapp, E.N., Dachev, T.P., Tomov, B.T., 2011. Statistical validation of HZETRN as a function of vertical cutoff rigidity using ISS measurements. Advances in Space Research 47, 600–610, http://dx.doi.org/10.1016/j.asr.2010.10.021.

40. Spurny, F., Dachev, Ts., 2003. Long-term monitoring of the onboard aircraft expo-sure level with a Si-diode based spectrometer. Adv. Space Res.32 (1), 53–58. http://dx.doi.org/10.1016/S0273-1177(03)90370-X.

41. Spurny, F., 2005. Response of a Si-diode-based device to fast neutrons. Radiat. Meas. 39, 219–223. http://dx.doi.org/10.1016/j.radmeas.2004.05.006.

42. Streb, C., Richter, P., Lebert, M., Dachev, T., Häder, D.-P., 2002. R3D-B, radiation risk radiometer-dosimeter on BIOPAN (Foton) and expose on the International Space Station (ISS). Proceedings of the Second European Workshop on Exo/Astrobiology, Graz, Austria, 16–19 September, (ESA SP-518), 71–74.

43. Uchihori, Y., Kitamura, H., Fujitaka, K., Dachev, T.P., Tomov, B.T., Dimitrov, P.G., Matviichuk, Y., 2002. Analysis of the calibration results obtained with Liulin-4J spectrometer–dosimeter on protons and heavy ions. Radiat. Meas.35, 127–134.

44. Uchihori, Y., H. Kitamura, N. Yasuda, H. Kentaro, K. Yajima, T.P. Dachev, Chapter 7: Liulin-4J portable Silicon Spectrometer, Results of the ICCHIBAN-3 and ICCHIBAN-4, Experiments to Inlercompare the Response of Space Radiation Dosimeters, HIMAC-128, NIRS, Japan, pp 76-88, March, 2008.

45. Vette, J.I., 1991. The NASA/National Space Science Data Center Trapped Radiation Environment Model Program (1964–1991). NSSDC/WDCA-R&S, pp. 91–92.

46. Wilson, J.W., Nealy, J.E., Dachev, T., Tomov, B.T., Cucinotta, F.A., Badavi, F.F., De Angelis, G., Leutke, N., Atwell, W., 2007. Time serial analysis of the induced LEO environment within the ISS 6A. Adv. Space Res.40 (11), 1562–1570. http://dx.doi.org/10.1016/j.asr.2006.12.030.

47. Wren, G.L., 2009. Chronology of 'relativistic' electrons: solar cycles 22 and 23. J. Atmos. Solar-Terr. Phys. 71, 1210–1218.

48. Zhang, L., Mao, R., Zhu, R., 2011. Fast neutron induced nuclear counter effect in Hamamatsu silicon PIN diodes and APDs. IEEE Trans. Nucl. Sci.58 (3), 1249–1256.

49. Zhao, H., and X. Li, 2013, Inward shift of outer radiation belt electrons as a function of Dst index and the influence of the solar wind on electron injections into the slot region, J. Geophys. Res. Space Physics, 118, 756–764, doi:10.1029/2012JA018179.

50. Zheng, Y., Lui, A.T.Y., Li, X., Fok, M.-C., 2006. Characteristics of 2–6 MeV electrons in the slot region and inner radiation belt. J. Geophys. Res. 111, A10204.

51. Zeitlin, C., 2014. Results from the MSL-RAD Experiment on the Curiosity Mars Rover, Nineteenth WRMISS, Krakow, Poland, 9-11 September 2014. http://wrmiss.org/workshops/nineteenth/Zeitlin_MSL-RAD.pdf

РАДИАЦИОННАТА ОБСТАНОВКА НА МЕЖДУНАРОДНАТА КОСМИЧЕСКА СТАНЦИЯ (МКС), КАКТО СЕ НАБЛЮДАВА ОТ ПРИБОРА R3DR2 ПРЕЗ ОКТОМВРИ-НОЕМВРИ 2014

Цв. Дачев, Б. Томов, Ю. Матвийчук, Пл. Димитров,
Н. Банков, Д.-П. Хедер, Г. Хорнек, Г. Райтц

Резюме

Космическата йонизираща радиация е изследвана с помощта на спектрометъра-дозиметъра R3DR2 по време на неговият полет извън руския модул "Звезда" на МКС през октомври-ноември 2014 г. Приборът е монтиран на платформата на ESA EXPOSE-R2. Приборът R3DR2 е разработен и използван за първи път по време на полета на платформата на ESA EXPOSE-R през 2009-2010 г. (Dachev et al., 2015a). Той е автоматизирано устройство с малко тегло и размер, което измерва видимата слънчева и ултравиолетова (UV) радиация в четири канала и йонизиращото лъчение в 256 канала със спектрометър на депозираната енергия от типа „Люлин" (Dachev et al., 2002). Основните резултати, получени от работата на R3DR2 са:

(1) открити са и са характеризирани количествено три различни източници на радиация - галактически космически лъчи (GCR), енергични протони от вътрешния радиационен пояс- (IRB) в района на Южно-атлантическата аномалия и енергични електрони от външния радиационен пояс (ORB);

(2) за първи път в историята на използването на спектрометри от тепа „Люлин" (Dachev et al., 2015a) е наблюдаван поток от слънчеви енергийни частици (SEP) в периода 1-4 ноември 2014;

(3) получените спектри на депозираната енергия са сравнени с други спектри и е потвърдена тяхната форма.